RNA exosome drives early B cell development via noncoding RNA processing mechanisms

Brice Laffleur, Carolina R. Batista, W Zhang, J Lim, Biao Yang, Delphine Rossille, L Wu, Jerson Estrella, Gerson Rothschild, Evangelos Pefanis, et al.

HHS Public Access

Author manuscript

Sci Immunol. Author manuscript; available in PMC 2022 August 07.

Published in final edited form as:

Sci Immunol. 2022 June 03; 7(72): eabn2738. doi:10.1126/sciimmunol.abn2738.

RNA exosome drives early B cell development *via* non-coding RNA processing mechanisms

Brice Laffleur[1,#,3], **Carolina R. Batista**[1,#], **Wanwei Zhang**[1,#], **Junghyun Lim**[1], **Biao Yang**[1], **Delphine Rossille**[3], **Lijing Wu**[1], **Jerson Estrella**[1], **Gerson Rothschild**[1], **Evangelos Pefanis**[2], **Uttiya Basu**[1,4,*]

[1]Department of Microbiology and Immunology, Vagelos College of Physicians and Surgeons, Columbia University, New York, New York 10032

[2]Regeneron Pharmaceuticals, Tarrytown, New York 10591

[3]Current address: Université of Rennes, INSERM, Etablissement Français du Sang Bretagne, Rennes, France.

[4]Lead contact

Abstract

B cell development is linked to successful V(D)J recombination, allowing B cell receptor (BCR) expression and ultimately antibody secretion for adaptive immunity. Germline non-coding RNAs (ncRNAs) are produced at immunoglobulin (Ig) loci during V(D)J recombination but their function and post-transcriptional regulation are incompletely understood. Trichohepatoenteric syndrome (THES) patients, characterized by RNA exosome pathway component mutations, exhibit lymphopenia, thus demonstrating the importance of ncRNA surveillance in B cell development in humans. To understand the role of RNA exosome in early B cell development in greater detail, we generated mouse models harboring a B cell specific *cre* allele (*Mb1*^{cre}), coupled to conditional inversion-deletion alleles of one RNA exosome core component (*Exosc3*) or RNase catalytic subunits (*Exosc10* or *Dis3*). We noticed increased expression of RNA exosome subunits during V(D)J recombination, while a B cell developmental blockade at the pro-B cell stage was observed in the different knock-out mice, overlapping with a lack of productive rearrangements of V(D)J genes at the *Ig* heavy chain (*Igh*). This unsuccessful recombination prevented differentiation into pre-B cells, with accumulation of ncRNAs and upregulation of the p53 pathway. Introduction of a pre-arranged *Igh* VDJ allele partly rescued the pre-B population in *Dis3*-deficient cells, although V-J recombination defects were observed at *Ig* light chain kappa (*Igκ*), preventing subsequent B cell development. These observations demonstrated that the RNA exosome complex is important for *Igh* and *Igκ* recombination and establish the relevance of RNA processing for optimal diversification at these loci during B cell development.

[*]Correspondence: ub2121@cumc.columbia.edu.
[#]Contributed equally

AUTHOR CONTRIBUTIONS

BL, CB and UB designed and interpreted the experiments, with critical input from JL. BL, CB and BY performed the experiments. WZ, BL, DR and CB analyzed the bioinformatics data. GR, JL and EP helped to develop mouse models. BL, CB and UB wrote the manuscript.

COMPETING INTERESTS

The authors declare no competing interests.

One Sentence Summary

The RNA exosome is crucial for B cell development.

INTRODUCTION

Adaptive immunity relies on the generation of new antigen receptors in T and B lymphocytes through V(D)J recombination, an antigen-independent recombination between variable (V), diversity (D), and joining (J) gene segments in the immunoglobulin (Ig) locus. Pro-B cells undergo D to J_H, followed by V_H to DJ_H recombination of their immunoglobulin heavy chain (*Igh*), inducing the expression of a pre-B cell receptor (pre-BCR) which provides survival and proliferation signals, and allows light chain rearrangement (1). In the immunoglobulin light chain loci (IgL), either Igκ or Igλ, recombination occurs in pre-B cells between V_L and J_L genes, inducing membrane expression of a functional B cell receptor (BCR), intracellular signaling, cell differentiation, and exit from the bone marrow and circulation in the periphery (2). These processes of gene rearrangement and cellular differentiation occur in distinct stages during B cell development and are critical to ensure a diverse B cell repertoire and high affinity antibody production.

Multiple mechanisms stringently regulate V(D)J recombination, including temporal and developmental-stage specific expression of the recombinases *Rag1* and *Rag2* (recombination activating genes), Ig gene positioning, chromosome organization, and open chromatin state (3). Ig genes undergo epigenetic changes before V(D)J recombination, including DNA demethylation, histone modification, and variations in DNase hypersensitivity. These changes open the chromatin to permit the RAG proteins access to the recombination signal sequences (RSS) (4). RAG is an evolutionarily conserved endonuclease which binds and cuts double-strand DNA. RAG structure (5) and mode of action (6) suggest that non-coding transcription could impede its DNA binding properties and cleavage activity if non-coding RNAs (ncRNAs) overlap RSS sites. Indeed, germline sense and antisense non-coding transcription is observed at different elements of *Ig* loci (7–9). Non-coding RNA processing and RNA surveillance also control loop extrusion mechanisms (10) implicated in RAG1/2 accessibility during V(D)J recombination (11–13). Finally, RAG1 protein is negatively regulated via sequestration in the nucleolus and accumulated nucleolar ncRNA could inhibit RAG1's Ig recombinational activity (14). Taken together, RNA surveillance of ncRNA could influence V(D)J recombination via multiple mechanisms.

RNA surveillance and non-coding decay are mediated by the RNA exosome, a multiprotein complex with 3' to 5' ribonuclease activity implicated in the processing and decay of various classes of RNAs in the nucleus (15) and DNA or chromatin-associated RNAs (10), (16), (17). The eukaryotic RNA exosome is composed of a catalytically inactive, nine essential subunit core which associates with 3' to 5' ribonucleases DIS3 and EXOSC10 in humans. Multiple myeloma (18, 19) and immunodeficiencies such as THES syndrome (20) have been associated with mutations in RNA surveillance genes, such as *DIS3* and *SKIV2L* in humans respectively, although their precise contributions in disease development remain to be elucidated.

The RNA exosome plays a fundamental role in degrading germline transcripts at repetitive and G-rich switch regions (necessary for class switch recombination (CSR)) during B cell activation, providing DNA accessibility to activation induced deaminase (AID) for optimal CSR (10, 21, 22). Here, we demonstrated that RNA exosome subunits were highly expressed during stages of antigen receptor loci diversification (both V(D)J recombination and CSR). The RNA exosome was required for B cell development from the pro-B cell to the pre-B cell stages and mediated processing of germline transcripts needed for V(D)J recombination.

Lack of RNA exosome activity led to defects during *Igh* locus recombination, impeding pre-BCR signaling, and consequently blocking B cell development at the pro-B cell stage. Failure of proper pre-BCR signaling in pro-B cells ultimately led to the activation of the p53 pathway. *Igk* locus recombination defects also were observed, suggesting that RNA exosome also contributed to the generation of VJ gene rearrangements and BCR expression in pre-B cells. Taken together, our study provides evidence that RNA exosome-mediated surveillance of non-coding transcripts is important during early B cell development.

RESULTS

Expression of RNA exosome subunits during early B cell development.

B cell development is initiated in the bone marrow where V(D)J genes undergo DNA recombination (3). Subsequent encounter with antigen triggers another round of *Ig* gene diversification by somatic hypermutation (SHM) and CSR during the germinal center (GC) reaction (23). Developing B cell populations are characterized by specific transcriptomic programs, which control the expression of the RAG recombinases and AID to initiate recombination. We asked whether expression of the RNA exosome subunits changes during early B cell development in the bone marrow by analyzing publicly available transcriptomic data from the Immunological Genome Project (ImmGen). RNA exosome subunits were expressed in all developing B cell sub-populations; however, we observed a higher expression of certain subunits including *Exosc3*, *Exosc10* and *Dis3* in GC B cells (Figure 1A). Higher expression levels in GC cells correlated with already described crucial functions of RNA exosome in CSR and SHM processes (10, 24, 25). In parallel, we also observed higher expression of most RNA exosome subunits in pro-/pre-B cells (Hardy fractions B and C; note: Hardy fractions define B cell precursors into subpopulations based on cell surface marker expression), found during V(D)J recombination both in adult bone marrow (postnatal immune system) (Figure 1A) and in fetal liver (prenatal immune system) (Figure S1A). To investigate the importance of these observations *in vivo* we developed dedicated mouse models to delete RNA exosome components in early B cell development using $Mb1^{cre}$ mice (26) in combination with *COIN* alleles for *Exosc3* (RNA exosome core subunit), *Exosc10*, or *Dis3* (RNA exosome catalytic subunits) (Figures S1B–S1D) (10, 24, 25). *COIN* heterozygous mice served as the reporter system; in these mice, one allele remains functional while GFP/RFP expression from the other allele depends on endogenous *Exosc3*, *Exosc10* or *Dis3* promoters after *cre*-mediated inversion of the *COIN* allele (Figures S1B–S1D). We found that heterozygous mice lacked a notable phenotype, as shown by the percentage of B splenocytes in $Mb1^{cre/+}$ $Dis3^{C/+}$ compared to $Mb1^{cre/+}$ $Dis3^{+/+}$ mice (Figure S1E). To confirm the expression of the RNA subunits *Exosc3*, *Exosc10* and *Dis3*

in B cells subsets present in the bone marrow, spleen, and Peyer's patches, we performed flow cytometry using a combination of known B cell development markers. We compared the levels of GFP/RFP expression, which are driven by *Exosc3*, *Exosc10* and *Dis3* gene promoters, as a readout for the expression of RNA exosome subunits in these cells. As expected, GFP/RFP reporter gene expression was noted at the pro-B cell stage in bone marrow, when *cre* recombinase was expressed and *COIN* alleles were inverted (Figure 1B). Developing pre-B and immature B cells continued to express GFP/RFP proteins in the bone marrow (Figures 1C–1E) before exiting to the periphery. Follicular B splenocytes were GFP/RFP positive and activated B cells from Peyer's patches also expressed *Exosc3*, *Exosc10,* and *Dis3* (Figures 1F and 1G). Consistent with transcriptomic data, we detected increased expression of *Exosc3*, *Exosc10* and *Dis3* specifically in bone marrow developing pro-B and large pre-B cells during V(D)J recombination and in activated B cells (Figures 1B, 1C, 1G and Figures S1F–S1H). We noted a distinct expression pattern for *Exosc10* which was also expressed during the transitional stages (Figure 1A) and in follicular B cells in the spleen (Figures 1A and 1F and Figure S1G, please see Figure S2A for schematic of B cell development). Expression of genes encoding RNA exosome subunits was observed in other cell types in a random manner, contrasting with the expression trend noted in B cells (Figures S2B–S2D). We also observed higher expression of other components of the RNA surveillance machinery, such as the RNA helicases *Ddx1*, *Ddx19a*, *Ddx41* and *Skiv2l* during early B cell development and in activated GC B cells (Figure S2E). Finally, motif enrichment analysis revealed common transcription factors (such as *Spi1*, *Spib* and others) binding sites located ~250bp upstream of the ATG sequences of *Exosc3*, *Exosc10,* and *Dis3* gene promoters explaining a similar co-regulation and co-expression profile observed in B cells (Figure S2F). Thus, our results suggest that RNA exosome subunit and cofactor expression can be temporally regulated during B cell development *in vivo*, and are notably increased during B cell developmental stages which are associated with antigen receptor gene diversification.

The RNA exosome supports the pro-B cell to pre-B cell transition and *Igh* rearrangement.

To evaluate the contribution of RNA exosome activity during B cell development, we used three B cell specific conditional knock-out mouse models harboring homozygous *COIN* alleles ($Exosc3^{COIN}$, $Exosc10^{COIN}$, $Dis3^{COIN}$). Flow cytometry analyses indicated that bone marrow developing B cells were blocked at the pro-B cell stage, whereas B cells were poorly able to differentiate into pre-B cells in the absence of *Exosc3*, *Exosc10,* and *Dis3* (Figure 2A and 2B). Bone marrow small pre-B cells and immature B cells consequently were decreased greatly (Figures 2C and 2D). Loss of RNA exosome subunits which led to the accumulation of pro-B cells in the bone marrow could be caused by an inability of pro-B cells to rearrange *Igh* genes. Indeed, *Igh* PCR assays detected a slight decrease in D to J_H recombination (Figure S3A), while V_H to DJ_H recombination was greatly decreased at V_HJ558 distal or V_H7183 proximal genes in the absence of the RNA exosome (Figures S3B to S3D).

To perform an accurate and unbiased quantification of the V(D)J recombination events in these cells, we sorted bone marrow pro-B cells and performed deep RNA-sequencing analysis. We reconstituted the Ig V(D)J sequences from RNA-seq data (using computational tool TRUST4) and performed a V-quest analysis using the international ImMunoGeneTics

information system (IMGT) database. These analyses reconstituted the unique V(D)J rearrangements from the RNA-seq data, and we normalized these unique rearrangements to the total number of reads. We were able to reconstitute 7,482 functional V(D)J junctions out of 648,140,008 reads in controls (11.55 per million reads) versus 1,326 functional V(D)J junctions out of 671,548,696 reads (1.98 per million reads) in DIS3-deficient pro-B cells, demonstrating a defect in V(D)J recombination in the absence of the RNA exosome, affecting the frequencies of both V_H and J_H gene usage (Figures 2E and 2F). By focusing on the productive rearrangements, the percentages/distribution of the different V_H family was not altered (Figure S3E). Chromatin regulation is associated with RNA exosome activity and RNA exosome sensitive ncRNAs (25, 27). However, chromatin accessibility in the *Igh* locus, as measured by ATAC-seq in sorted pro-B cells ($B220^+$ $CD43^+$ IgM^-), remained unchanged (Figures S3F and S3G), suggesting that this defect is not due to a lack of open chromatin but rather to the accumulation of non-coding transcripts in the absence of DIS3. Repertoire analyses revealed a decrease in CDR3 length in cells lacking RNase activity, suggesting that RNA processing is necessary for accurate V(D)J junctions (Figure 2G). Taken together, our findings highlight a role for RNA exosome in early B cell development via mechanisms that involve antigen receptor locus recombination.

B cell development is affected by the deletion of RNA exosome subunits.

Despite the strong block in B cell development at the pro-B stage, a small percentage of B cells were able to exit the bone marrow and migrate into the periphery, populating the spleen and Peyer's patches. Flow cytometry analyses showed that follicular B cells were substantially affected by the absence of the RNA exosome subunits (Figures 3A and 3B). In contrast, the percentages of marginal zone (MZ) B cells were not significantly decreased (Figures 3A and 3C). This leads to higher MZ/follicular B cell ratios in the absence of RNA exosome activity (Figure 3D). In the gut-associated lymphoid tissue Peyer's patches, both resting and activated B cells were decreased in the absence of the RNA exosome catalytic subunits (Figures 3E–3G). We also compared RNA exosome-proficient versus RNA exosome-deficient mice by combining all the RNA exosome-deficient genotypes (*Exosc3*, *Dis3* and *Exosc10*) and confirmed the accumulation of pro-B cells and the consequent decrease of other B cell subsets. In addition, we noted an altered MZ/follicular ratio (Figures S4A–S4C). Further independent experiments confirmed the altered MZ/follicular ratio in the absence of *Dis3* (Figures S4D and S4E). Collectively, these data suggest that the functionality of RNA exosome degradation machinery is not restricted to the early developmental stages where B cell precursors are recombining their *Ig* genes. RNA exosome activity potentially is required for regulating the expression levels of genes controlling fate decision as B cells enter the follicles or the marginal zone in the secondary lymphoid organs.

Dis3 deletion leads to an accumulation of non-coding transcripts and upregulation of the p53 pathway.

To determine whether non-coding RNA accumulation could occur during defective B cell development in RNA exosome-deficient B cells, we investigated the transcriptome of $Mb1^{cre/+}$ $Dis3^{C/C}$ pro-B cells. The transcriptome from RNA exosome-deficient cells is a robust tool for detecting transiently expressed non-coding RNAs that are normally expressed

but difficult to detect in RNA exosome-proficient cells (10, 24, 25). We validated efficient depletion of *Dis3* mRNA *in vivo* in homozygous cells (Figure S5A) and analyzed DIS3-sensitive RNA substrates. In bone marrow derived developing pro-B cells, long non-coding RNAs (lncRNAs, Figure 4A), intergenic and intragenic enhancer-associated RNAs (eRNAs, Figure 4B), and antisense transcription start site at promoters (aTSS-RNAs, Figure 4C) have altered expression, and were perturbed genome-wide (Figure 4D). We also confirmed accumulation of antisense RNAs (asRNAs) while messenger RNA (mRNA) levels were not pervasively perturbed (Figure 4D), consistent with our previous observations in activated B cells (10, 24, 25). We showed multiple examples of ncRNAs, including aTSS-RNAs, antisense RNAs in gene bodies (Figures S5B and S5C), and eRNAs (Figure S5D) which were sensitive to DIS3 activity. RNA exosome deficiency did not reduce the expression of pro-B cell essential genes, like *Irf4*, *Il7r* or the *Rag1/2* recombinases (Figures S5B, S5C, and S5E), while ncRNAs consistently accumulated at different regions of the genome (Figure S5F).

Non-coding transcription at *Ig* genes during V(D)J recombination (9) correlates with chromatin accessibility to the transcription and recombination machineries (3, 4). The processing machinery of *Ig* locus/V(D)J recombination-associated ncRNAs is known, however direct implication of ncRNAs in V(D)J recombination events has not been evaluated thus far. By focusing our RNA-sequencing analysis specifically on the *Igh* locus, we observed an increase in antisense germline transcription overlapping J_H (Figure 4E) and D genes (Figure 4F), potentially impeding the first step of D to J_H recombination (Figure S3A). While we observed weak germline non-coding transcription at V_H genes in control cells, we found a significant accumulation of ncRNAs spread over all the V_H genes in the absence of RNA exosome activity (Figures 4G–4I). These transcripts were mainly antisense ncRNAs overlapping RSS and V_H genes (Figures 4G, 4H and Figures S6A–S6D) that may interfere with RAG binding, cleavage and/or accessibility at these recombination sites. Notably, we showed an inverse correlation between ncRNA accumulation and decreased coding of V_H expression in the absence of DIS3 (Figure S6E). These data suggest that *Igh* germline transcription is sensitive to DIS3 activity and in the absence of ncRNA processing V(D)J recombination at *Igh* loci is decreased.

Next, we analyzed differentially expressed genes in pro-B cells (Figure S6F and Table S1) and evaluated overall impact of the RNA exosome in pro-B cell biology by performing gene set enrichment analysis. Affected KEGG pathways were related to pro-B cell maturation including hematopoietic cell lineage or MAPK signaling pathways, for example (Figure 4J). DIS3-deficient cells have increased expression of p53 pathway-associated genes (Figure 4J), leading to programmed cell death in order to avoid the accumulation of pro-B cells harboring unproductive V(D)J recombination (28) along with mRNA expression perturbations and/or DNA damage response (25). We showed the increased expression of *Trp53* (Figure 4K) and associated genes from RNA-seq data (Figure 4L). We performed independent experiments to confirm the increased expression of the p53 pathway-associated genes observed in the RNA-seq data (Figure S6G) by RT-qPCR. Increased expression of p53 pathway-associated genes, ultimately led to apoptosis in the absence of DIS3 and ncRNA processing (Figure S6H). These observations corroborate the pro-B cell blockade phenotype and pre-B cell differentiation defect in the absence of RNA exosome. Of note, V(D)J

recombination components themselves (including *Rag* recombinases expression) and related pathways were not affected in DIS3 deficient cells. Taken together, these results suggest that the V(D)J recombination defect in the absence of DIS3 is not caused by abnormal gene expression of V(D)J recombination regulatory pathways, as deregulated pathways in DIS3-deficient B cells were not related to DNA recombination or programmed DNA repair themselves (Figure 4J). Rather, our data reveal genome-wide accumulation of ncRNAs (Figure 4D), especially of germline transcripts at the *Ig* loci (Figures 4E–4I), raising the possibility of a crucial role of the RNA exosome in the regulation of expression of ncRNAs enabling proper V(D)J recombination.

A rearranged *Igh* allele rescues pro-B to pre-B cell differentiation.

Defects in V(D)J recombination can be rescued using a pre-arranged TCR/BCR, even in the absence of RAG recombinases (29). We introduced a pre-arranged *Igh* V(D)J gene, i.e. $V_HB1–8$ allele (30) (Figure 5A, S7A) in the $Mb1^{cre}$ $Dis3^{COIN}$ mice to evaluate a potential rescue in B cell development in the absence of RNA exosome activity. We confirmed an efficient deletion of the *Dis3 COIN* alleles in the $V_HB1–8^{KI/KI}$ $Mb1^{cre/+}$ $Dis3^{COIN}$ B splenocytes. First, we used flow cytometry to directly visualize *Dis3* relative expression. $V_HB1–8^{KI/KI}$ $Mb1^{cre/+}$ $Dis3^{C+/}$ B cells demonstrated expression of GFP (i.e. *Dis3*), in experiments using $V_HB1–8^{KI/KI}$ $Mb1^{cre/+}$ $Dis3^{+/+}$ B cells as control (Figure 5B). Indeed, $V_HB1–8^{KI/KI}$ $Mb1^{cre/+}$ $Dis3^{C/C}$ have stronger GFP expression than heterozygous cells, as would be predicted on the basis of two $Dis3^{COIN}$ inverted alleles (Figure 5B). We sorted B cells, and qPCR quantification confirmed a robust deletion of the $Dis3^{COIN}$ allele, specifically in B cells expressing a *cre* recombinase, with ~50% of deletion in heterozygous cells and ~95% of deletion in homozygous cells (Figure S7B). These data suggest that a fraction of B cells was able to develop efficiently in the absence of DIS3 when they express a knock-in transgenic BCR and restore the small pre-B cell population.

In these conditions $V_HB1–8^{KI/KI}Mb1^{cre/+}$ $Dis3^{C/C}$ B cells were able to differentiate to a similar level as $V_HB1–8^{KI/KI}$ $Mb1^{cre/+}$ $Dis3^{C/+}$ progenitors from the pro-B to the small pre-B stage (Figures 5C and 5D), suggesting the role of the RNA exosome complex in V(D)J recombination and subsequent differentiation into pre-B cells. In this model, V_L to J_L recombination is dependent on endogenous *Igl* genes in pre-B cells. Thus, in the absence of IgL rescue, the subsequent differentiation into immature B cells was reduced in bone marrow (Figures 5C and 5D), with fewer peripheral B cells observed in spleen in the absence of DIS3 (Figures S7C and S7D). Additionally, the MZ/follicular B cells ratio was also higher in this $V_HB1–8^{KI/KI}$ $Mb1^{cre/+}$ $Dis3^{C/C}$ model (Figure S7E).

Collectively, these results directly demonstrated RNA exosome's function in V(D)J recombination specifically during the pro-B to pre-B transition.

Dis3 deletion leads to decreased recombination in the *Igκ* light chain.

While pro-B cells are differentiating from lymphoid progenitors with *Igh* genes accessible and primed to undergo V(D)J recombination, *Igκ* recombination depends on successful recombination and expression of the pre-BCR. To understand whether open chromatin (accessibility) of the *Igκ* locus is widely affected in DIS3-deficient B cells, we performed

ATAC-seq assays in sorted pro-B cell populations. Genome-wide analyses reveal a selective impact of DIS3 loss on chromatin accessibility, with more than 6,000 peaks decreased in the absence of RNA processing and fewer than 1,000 peaks showing increased accessibility (Figures S8A and S8B and Table S2). 175 peaks were decreased at CTCF-binding elements (CBEs) while only 7 were increased; 162 peaks showed less accessibility at promoters while 175 peaks gained accessibility. These differences in accessibility could reflect different maturational stages, with DIS3-proficient cells prone to differentiate while DIS3-deficient cells are blocked at the pro-B stage. Finally, 606 peaks were decreased at enhancer regions, but no gains were observed at enhancers (Figure S8C). We evaluated DNA accessibility at the *Igκ* alleles in DIS3-proficient versus DIS3-deficient cells and observed decreased accessibility in some parts of this locus. However, the majority of *Igκ* still had open chromatin (Figure 6A). Thus, chromatin accessibility was mostly intact during *Vκ* to *Jκ* gene rearrangements in DIS3-deficient B cells. In contrast, *Vκ* recombination was decreased across the *Igκ* locus in DIS3-deficient B cells (Figures 6B and 6C). Total productive *Igk* rearrangements were decreased from 4,566 functional VκJκ junctions out of 648,140,008 reads in controls (7.05 per million reads) to 933 out of 671,548,696 reads (1.39 per million reads) in the absence of DIS3, approximately a factor of 5 (Figures 6B and 6C), but *Igλ* recombination level was affected only from 207 functional VλJλ junctions out of 648,140,008 reads in controls (0.32 per million reads) to 98 out of 671,548,696 reads (0.15 per million reads), approximately a factor of 2, (Figures 6D and 6E), resulting in a higher proportion of *Igλ* recombination (Figure 6F) in our repertoire analysis. Of note, *Vk* and *Vλ* usages were not skewed (Figures S8D and S8E). As previously mentioned, $V_HB1\text{–}8^{KI}$ mice harbor a prearranged V(D)J gene and still have to recombine the Ig light chain to develop immature and mature B cells. We evaluated *Igκ* recombination in these cells by flow cytometry and again found fewer $Ig\kappa^+$ mature B cells in the periphery compared to the control (Figures 6G and 6H). Taken together, our data revealed a critical contribution of DIS3 to successful recombination of *Igk* genes, while *Igλ* was less affected.

DISCUSSION

The RNA exosome complex has critical functions during B cell activation, including (a) critical regulation of ncRNAs overlapping switch sequences, (b) giving accessibility to both DNA strands for AID-mediated cytidine deamination for efficient CSR (21, 22, 24), and (c) by controlling chromosomal architecture (10). Outside the *Igh* locus, super-enhancer-associated RNA exosome-sensitive ncRNA transcription recruits AID activity causing oncogenic mutations (24, 25). In agreement with these important functions, expression profile analyses of RNA exosome complex subunits demonstrated enhanced expression in the germinal center. Strikingly, we found that RNA exosome subunit expressions are also increased during V(D)J recombination in immature bone marrow B cells, piquing our interest in their function in early B cell development. Our observations indicate an evolutionarily designed mechanism to co-regulate the expression of the different RNA exosome subunits during two crucial steps of B cell development.

We observed that some of the RNA exosome subunit promoters share common transcription factor binding sites, suggesting their concomitant regulation in B cells whereas other, additional regulatory elements potentially add function in a cell-specific manner. Most of

the RNA exosome subunits also have increased expression in B1a B cells in the spleen. B1a B cells are long-lived, self-renewing innate-like B cells, and have potential implications in viral clearance (31), suggesting that increased expression of the RNA exosome subunits could be implicated in anti-viral immunity, potentially by directly degrading viral RNAs (32). RNA exosome-deficient mice have a severe defect in B cell development, with B cell accumulation at the pro-B cell stage. Consequently, development of peripheral follicular B cells is strongly affected because RNA exosome-deficient B cells cannot migrate and survive in the periphery. However, we observe normal MZ B cell compartments. These differences in follicular B cells versus marginal zone B cells could be due to differences in the kinetics of RNA exosome subunit deletion in our mouse model or could be a due to a more mechanistic and biological reason that we do not yet understand.

Tonic BCR signaling controls B cell fate, with low tonic signaling usually favoring MZ differentiation (2, 33). We observed weak expression of the BCR in the absence of the RNA exosome, and postulate that this arises due to a suboptimal 3D configuration of the *Igh* locus and accumulation of ncRNAs at the 3'RR and Eμ enhancers, with Eμ controlling heavy chain expression (34). Thus, it is possible that weak BCR expression induces low tonic signaling and promotes MZ B cell differentiation in our models. Further investigation will determine how the RNA complex could specifically regulate B cell fate and whether its activity is more dispensable for MZ B cells. We sequenced the non-coding transcriptome from primary pro-B cells in which *Dis3* gene deletion was very efficient *in vivo*. In activated B cells, lncRNAs, eRNAs, aTSS-RNAs, and antisense RNAs are DIS3 substrates (10). The RNA exosome has the ability to degrade these categories of ncRNAs ubiquitously (independent of the cell type), while specific functions are ensured by distinct expression patterns of RNA exosome sensitive-ncRNAs (i.e. germline ncRNAs at V_H genes, or germline ncRNAs at switch regions).

A complete understanding of the interplay between RNA processing and chromatin modifications remains elusive, although circumstantial evidence indicates that chromatin-associated RNAs can influence epigenetic and transcriptional outcomes (17, 35–38). Chromatin-associated lncRNAs also have been shown to function in CTCF site regulation and local chromosomal architecture (39). In developing pro-B cells, we observed a moderate impact of RNA exosome mediated RNA processing on chromatin accessibility, with both *Igh* and *Igκ* having strong recombination defects but mild effects on ATAC-seq-measured chromatin accessibility in DIS3-deficient cells.

Accessibility at promoter sequences was variable, with gain and loss, possibly because of different differentiation stages. Enhancer-expressed ncRNAs (eRNAs) (40) are processed by the RNA exosome (25). In the absence of RNA processing we observed an accumulation of eRNAs along with decreased chromatin accessibility at some enhancers, while almost no gain was seen, suggesting that ncRNA accumulation at enhancers mostly leads to decreased accessibility. The RNA exosome is associated with transcription elongation and termination (41, 42) and chromatin accessibility at enhancers could be perturbed by an alteration of RNA polymerase II configuration at these sites. However, widespread effects on chromatin accessibility may not occur following RNA exosome deficiency or are not observable in our *in vivo* model systems due to experimental limitations.

We demonstrated that DIS3 regulates germline transcripts, strongly expressed during V(D)J recombination, and normally processed by the RNA surveillance machinery. Many factors contribute to and regulate V(D)J recombination including RSS sequences composition, chromatin accessibility, epigenetic chromatin marks, transcription factor binding, chromatin architecture protein occupancy (including cohesin and CTCF), or sense and antisense transcription (43, 44). We propose now that RNA processing of ncRNAs by the RNA exosome and its cofactors is an important additional requirement for optimal V(D)J recombination.

It seems non-coding transcription could be critical for appropriate chromatin structure and nucleosome positioning (45) before V(D)J recombination. RNA exosome-deficient cells tend to accumulate chromatin-associated RNAs (10, 16) which may interfere with RAG1/2 DNA binding necessary for catalysis of DNA breaks at RSS sequences. Decreased V(D)J recombination in the absence of DIS3 may explain why V(D)J recombination can occur in the absence of transcription (46–48), as germline transcription is likely a consequence of accessible chromatin but is not absolutely required for recombination. We propose that germline ncRNAs might be resolved by the RNA processing machinery to complete this process. To reach a definitive conclusion on the impact of RNA exosome deficiency on V(D)J recombination we rescued the developmental defect at the pro-B/pre-B cell transition by introducing a pre-arranged *Igh* $V_HB1–8$ allele. Notably, the expression of this transgenic V(D)J allele partly restores normal levels of pre-B cells. While RNA exosome activity could control many other aspects of the pro-B to pre-B cell transition, this rescue experiment clearly suggests a direct implication of the RNA exosome complex in V(D)J recombination. Moreover, alteration of CDR3 length also suggests that ncRNA processing is necessary to generate physiological CDR3 junctions, while chromatin associated ncRNA and/or RNA:DNA hybrids accumulation eventually interferes with the DNA repair machinery (25, 49).

While cellular proliferation could be affected in the absence of DIS3 it is unlikely to impact RAG-mediated DNA breaks and DNA repair which occur in non-proliferative pro-B cells. RAG scanning during V(D)J recombination is dependent on chromatin loop extrusion mediated by CTCF binding at CBEs in concert with cohesin translocation on the Ig loci (11–13). DIS3 deficiency leads to an accumulation of chromatin-associated ncRNAs along with disorganized cohesin localization in activated B cells, thus ncRNA transcription and processing that may generate non-B DNA structures are possible mechanisms for regulating loop extrusion kinetics (10). It is possible that a similar mechanism due to aberrant ncRNA accumulation interferes with physiological loop extrusion kinetics during V(D)J recombination and RAG scanning, thereby impeding RAG-mediated DNA cleavage and V(D)J recombination in the absence of the RNA exosome. These possibilities will be experimentally tested in future studies.

Finally, we consider the pathological consequence of RNA exosome function deficiency in humans where mutations in the RNA helicase *SKIV2L* (an RNA helicase cofactor of the RNA exosome complex) have been associated with THES syndrome (20), a rare disease characterized by immunodeficiency and very low antibody titers. A mouse model demonstrates that THES2-like phenotypes can be created successfully by specifically

deleting *Skiv2l* during early B cell development, using the same $Mb1^{Cre/+}$ mice crossed with *Skiv2l* floxed alleles (shown in the companion manuscript (50)). THES2 patients demonstrate inflammatory responses and a lack of antibody production, but the molecular explanation of antibody deprivation is unknown. Following *Skiv2l* deletion through specific flox targeting and *cre*-expression in pro-B cells, a developmental defect similar to what we report in core RNA exosome knockout mouse models is observed. However, SKIV2L depletion in mature B cells did not cause class switching defects (50). SKIV2L activity is primarily important for supporting RNA exosome-mediated co-translational decay of mRNAs in the cytoplasm (51) by extracting mRNA from stalled 80S ribosomes (52) and this activity has been validated at a structural level (53). Moreover, in SKIV2L mutant immature B cells, nuclear non-coding RNA stabilization was not observed. Thus, SKIV2L action may indirectly promote nuclear exosome localization and function during early B cell development by keeping the cytoplasmic RNA exosome pool active.

In this study, we show that core RNA exosome component loss leads to a developmental defect in immature B cells similar a to previous study where we showed its function in mature B cells and class switch recombination (24). During CSR, the accompanying RNA helicase is MTR4, a component of the NEXT complex that unwinds RNA/RNA and DNA/RNA hybrids in the nucleus to facilitate *Igh* DNA recombination (22, 54). Thus, the core RNA exosome functions with different RNA helicases and associated complexes during different steps of *Igh* recombination, namely with the MTR4/NEXT and other nuclear helicases during CSR and indirectly via the SKI complex during early B cell development. Discovery and characterization of RNA exosome-associated specific nuclear helicases and other cofactors during V(D)J recombination will be important steps forward in understanding the role of ncRNA processing during V(D)J recombination.

MATERIAL AND METHODS

Study Design

This study aimed to understand the role of non-coding RNA processing during the early steps of B cell development and the processes of V(D)J recombination. We developed dedicated mouse models to dissect the functions of the RNA exosome complex, allowing genetic deletion in pro-B cells ($Mb1^{cre/+}$) of one core subunit gene (*Exosc3*) or the catalytic subunit genes (*Exosc10* and *Dis3*), and another model ($V_HB1\text{–}8^{KI/KI}$) to rescue the observed developmental blockade at the pro-B cell stage. These mice were analyzed by flow cytometric analyses and deeper investigation of ncRNA accumulation were performed through RNA-sequencing while chromatin accessibility was evaluated by ATAC-sequencing.

Mice

$Mb1^{cre/+}$ mice (26) were obtained from Prof. Michael Reth (University of Freiburg). $V_HB1\text{–}8^{high}$ knock-in mice (named in this study $V_HB1\text{–}8^{KI/KI}$) (30) were provided by Prof. Michel Nussenzweig (Rockefeller University). *Exosc3*, *Exosc10*, and *Dis3 COIN* alleles have been previously described (10, 24, 25)), and are presented in Figures S1B–S1D. We used heterozygous mice as control (e.g. $Dis3^{COIN/+}$, named as $Dis3^{C/+}$) and homozygous mice as conditional KO (e.g. $Dis3^{COIN/COIN}$, named as $Dis3^{C/C}$).

8 to 12 weeks male and female mice were used for experiments. Mice experiments were approved by the Columbia University IACUC committee and performed following the recommended guide line of Columbia University (protocol number AC-AABP7556).

Flow cytometry and cell sorting

Bone marrow, spleen, and Peyer's patches were collected from the different mice, red blood cells were removed by hypotonic lysis (ACK buffer) from bone marrow and spleen, before saturation in FACS buffer with Fc block (clone 2.4G2, BD Biosciences 553141) for 10 minutes at room temperature. Then cells were stained with antibodies for 30 minutes at 4°C in FACS buffer (PBS with 3% FBS), washed, and analyzed.

To study B cell development of *Exosc3*^{COIN}, *Dis3*^{COIN} mice (both expressing GFP after *COIN* alleles inversion), and $V_HB1\text{–}8^{KI/KI}$ mice we used the following panel of antibodies: anti-B220 BV510 (clone RA3–6B2, BD Biosciences 557683), anti-CD43 PE (clone S7, BD Biosciences 553271), anti-CD25 APC (clone PC61, BD Biosciences 557192), anti-IgM PE-Cy7 (clone R6–60.2, BD Biosciences 552867), anti-CD21 APC (clone 7E9, BioLegend 123411), anti-CD23 PE (clone B3B4, BD Biosciences 553139), anti-GL7 PE (clone GL7, eBioscience 12–5902-82), anti-Igk V450 (clone 187.1, BD Biosciences 561354), anti-CD19 APC (clone 1D3, BioLegend 115530). Live cells were gated as lymphocytes and single cells; dead cells were stained with 7AAD or DAPI and excluded from the analyses.

For B cell development analyses of *Exosc10*^{COIN} mice (expressing RFP after *COIN* allele inversion), the same panel of antibodies was employed, substituting anti-B220 Alexa 700 (clone RA3–6B2, BD Biosciences 557957), anti-CD43 FITC (clone S7, BD Biosciences 553270), anti-CD23 FITC (clone B3B4, BD Biosciences 561772), anti-GL7 FITC (clone GL7, BD Biosciences 562080). Live cells were gated as lymphocytes and single cells; dead cells were stained with DAPI and excluded from the analyses. For CD19 cell sorting we used anti-CD19 PerCP-Cy5.5 (clone 6D5, BioLegend 115533). Data were acquired on Fortessa, LSR2 or Accuri C6 (BD) machines with subsequent analysis using FlowJo software, and cell sorting was performed on Aria II (BD).

PCR and qPCR

For DNA extraction, cells were suspended in proteinase K buffer with proteinase K and incubated overnight at 56°C. Genomic DNA was extracted by ethanol precipitation, washed in 70% ethanol and suspended in TE buffer. Bone marrow cells were employed to evaluate the usage of the different V_H family of genes (distal V_HJ558 versus proximal V_H7183) and D to J_H3 recombination.

PCR was performed on 100 μg, 10 μg and 1 μg of genomic DNA using the following primers: V_HJ558 for gcgaagcttargcctgggrcttcagtgaag and J_H4 rev aggctctgagatccctagacag; V_H7183 for cggtaccaagaasamcctgtwcctgcaaatgasc and J_H4 rev aggctctgagatccctagacag; D for aggctctgagatccctagacag and J_H3 rev gtctagattctcacaagagtccgatagaccctgg as previously described (55, 56). As loading control, Cμ primers: Cμ for tggccatgggctgcctagcccgggactt and Cμ rev gcctgactgagctcacacaaggagga.

qPCR was performed on genomic DNA from $CD19^+$ and $CD19^-$ sorted splenocytes. For *Dis3 COIN* allele inversion the following primers were used: $Dis3^{COIN}$ for caaggaaaccctggactactg and $Dis3^{COIN}$ rev aatgggtctagcacatgcacatc; the qPCR signals were normalized using *Myc* primers: *Myc* for agcgcagcatgaattaactgc, *Myc* rev gtatacgtggcagtgagttg. qPCR was performed on 50 ng of gDNA using SYBR Green and Roche Lightcycler II apparatus.

RNA extraction, cDNA synthesis, and qPCR

Total RNA was extracted from FACS-sorted pro-B cells from $Mb1^{+/+}$ $Dis3^{C/C}$ and $Mb1^{cre/+}$ $Dis3^{C/C}$ mice using the RNeasy Mini Kit (QIAGEN). cDNA was synthetized using Oligo DT primers and SuperScript IV Reverse Transcriptase (Thermo Fisher Scientific). qPCR was assembled using Maxima SYBR Green Mix (2X) (Thermo Fisher Scientific) in triplicates. Gene expression levels were normalized by GAPDH and gene expression levels for individual genes are presented as 2^-(Delta CT), using the following oligonucleotides:

Bbc3 for (gtgaccactggcattcattg), Bbc3 rev (ctcctccctcttctgagactt),

Cdkn1 for (ctggtgatctgctgctcttt), Cdkn1 rev (ccctgcatatacattcccttcc),

Bax for (ggagatgaactggacagcaata), Bax rev (gaagttgccatcagcaaacat),

Trp53 for (aagatccgcgggcgtaa), Trp53 rev (catcctttaactctaaggcctcattc),

GAPDH for (acttcaacagcaactcccactcttc), GAPDH rev (tccagggtttcttactccttggag).

RNA sequencing

Bone marrow were collected from mice, red blood cells were removed by hypotonic lysis (ACK buffer) and cells were saturated in FACS buffer (PBS with 3% FBS) with Fc block (clone 2.4G2) for 10 minutes at 4°C. Then cells were stained with antibodies for 30 minutes at 4°C in FACS buffer, washed, and pro-B cells were sorted as $B220^+$, $CD43^+$, $CD25^-$, IgM^-, live singlet cells using a BD Aria cell sorter. RNA was extracted using TRIzol (Invitrogen™ TRIzol™ Reagent), RNA quality was evaluated by Bioanalyzer (Agilent) and RNA samples were sequenced using the RNA Ribozero 90M 100PE sequencing kit (Illumina) at the Columbia University Genome Center.

Chromatin Accessibility Assay (ATAC-Seq)

Bone marrow preparations from two $Mb1^{cre/+}$ $Dis3^{C/+}$ and $Mb1^{cre/+}$ $Dis3^{C/C}$ littermate mice were FACS-sorted to isolate the pro-B cell population ($B220^+$ $CD43^+$ IgM^-). An average of 100,000 pro-B cells were isolated from each mouse. Nuclei isolation and transposition was performed as previously described in the Omni-ATAC protocol (57). The total of four samples had libraries synthetized using NEBNext® High-Fidelity 2X PCR master mix with Nextera transposase adapter primers containing different indexes. Indexed libraries were multiplexed before and pair-ended sequenced using an Illumina NextSeq instrument.

Statistical Analysis

Statistical analyses were performed using GraphPad Prism software, including two-tailed *t*-tests (paired or unpaired), and two-tailed proportion tests (Khi2) ns = non-statistically significant; * *P*-value < 0.05; ** *P*-value < 0.01; *** *P*-value < 0.001; **** *P*-value < 0.0001.

Bioinformatic analyses

RNA exosome subunits expression.—The expression levels of the RNA exosome subunits were extracted from the "ImmGen data browsers microarray" (http://www.immgen.org), and the values were plotted as heat maps.

Motif enrichment (MEME) analysis.—Motif enrichment analysis was performed using MEME Suite 5.4.1. Sequence regions 250 base pairs upstream of ATG were retrieved for *Dis3* (chr14:99,099,669–99,099,907), *Exosc3* (chr4:45,320,580–45,320,829) and *Exosc10* (chr4:148,558,216–148,558,471) genes. The following settings were used for motif discovery: Motif discovery mode, classic mode; selected site distribution, any number of repetitions; number of motifs, 3.

Data processing.—We use RTA (Illumina) for base calling and bcl2fastq2 (version 2.17) for converting BCL to fastq format, coupled with adaptor trimming. The resulting reads were mapped to mm9 genome of house mouse by hisat2 (version 2.1.0) (58) with default parameters. We used StringTie (version 1.3.3b; parameter "--rf") (59) for transcript assembly and expression quantification. The read/fragment counts of features were quantified by FeatureCounts and the differential features were detected by DEseq2 with criterion of fold change ≥2 and FDR <0.05. For visualization in IGV, we merged bam files from replicates by Samtools and generated normalized and strand-specific bedgraph files using Bedtools and properly calculated scaling factors. The bedgraph files were then converted to bigwig by bedGraph2bigWig utility from UCSC. For RNA-seq, we used depth-1x normalization method which normalized the sequencing depth to 1x coverage. For ATAC seq, we use RPM (reads per million mapped reads) normalization.

Differential analysis of lncRNA, eRNA and aTSS-RNA.—lncRNAs that do not overlap with protein-coding exons and with length larger than 200nt were collected. These RNAs were merged across all samples if they overlapped with each other. The merged transcripts were re-quantified using FeatureCounts (parameter "-s 2 -p") to obtain the fragment counts table. DEseq2 was applied to the fragment counts table to obtain the differentially expressed lncRNAs (fold change>=2 and FDR<0.05). These lncRNAs were shown in the heatmap of FPKM. We collected non-coding RNAs that overlap with enhancer regions as enhancer RNA (eRNA). The enhancer regions were defined by H3K27Ac and H3K4me1 markers from public ChIP-seq (GSM2184223 and GSM2184242). The aTSS-RNA expression was quantified as the non-coding RNA expression in the anti-TSS region (within 2kb upstream of TSS but in the antisense strand). The differentially expressed eRNAs and aTSS-RNAs were selected with the same strategy as in the situation of the lncRNA and also are shown in the heatmaps.

Pathway enrichment analysis.—The up- and down-regulated gene sets were submitted to DAVID (60) for KEGG pathway enrichment analysis. The -log10(P-value) of each significant (P-value<0.05) pathway is shown in the bar graph.

Immune repertoire reconstruction analysis.—TRUST4 (61) with parameters "--abnormalUnmapFlag" was used to reconstruct the immune repertoire.

ATAC-sequencing analysis.—Raw sequencing reads were subjected to adapter trimming by Cutadapt (62) with parameters "--trim-n -q 5,5 -m 20 -e 0.1". The resulting reads were mapped to the reference genome of mm9 by bowtie2 (63) (version 2.2.9) with parameter "-k 4 -X 2000 --local". Duplicate, multi-mapped reads and reads that mapped to mitochondria were removed. Peak calling was performed using MACS2 (64) (parameter "--nomodel --shift −100 --extsize 200 --broad -f BAMPE"). Bigwig files with RPM (reads-per million-mapped) normalization were generated for visualization via the IGV or UCSC genome browsers. The peaks across all samples were merged and quantified by featureCounts to obtain the read count table. DEseq2 was used to identify the differential peaks. ATAC signals around the summit of differential peaks were plotted in white-blue heatmap.

Supplementary Material

Refer to Web version on PubMed Central for supplementary material.

ACKNOWLEDGMENTS

We thank Prof. Michel Nussenzweig (Rockefeller University) for providing V_HB1–8 mice, Prof. Michael Reth (University of Freiburg) for $Mb1^{cre}$ mice and members of the Basu laboratory and numerous colleagues for very important scientific input. We thank the Columbia University Flow Cytometry Core of the Stem Cell Initiative and Department of Microbiology and Immunology cell sorting facility (both for FACS and cell sorting) and the Columbia University Genome Center (for high throughput genomics).

FUNDING

Research in the Basu lab is supported by grants: B.L. (EMBO fellowship, ALTF 906–2015) and U.B. (1R01AI099195, 1RO1 AI143897–01A1 and R01AI134988), Leukemia & Lymphoma Society, and the Pershing Square Sohn Cancer Research Alliance.

DATA AND MATERIAL AVAILBILITY

All raw sequencing data can be obtained from NIH bioproject with the accession number PRJNA774248. The processed data (bigwig and/or broadpeak) of RNA-seq and ATAC-seq can be obtained from http://52.20.87.23/public/VDJ_project/. Codes related to the analysis are available in https://github.com/basulab-cu/VDJ_project. We also reused these codes https://github.com/basulab-cu. The mouse models used in this study to conditionally delete subunits of RNA exosome can be obtained following completion of a Biological Material Transfer Agreement with Columbia University and Regeneron Pharmaceuticals. All data needed to evaluate the conclusions in the paper are present in the paper or the Supplementary Materials.

References and notes

1. Herzog S, Reth M, Jumaa H, Regulation of B-cell proliferation and differentiation by pre-B-cell receptor signalling. Nat Rev Immunol 9, 195–205 (2009). [PubMed: 19240758]
2. Yam-Puc JC, Zhang L, Zhang Y, Toellner K-M, Role of B-cell receptors for B-cell development and antigen-induced differentiation. F1000Research 7, 429 (2018). [PubMed: 30090624]
3. Schatz DG, Ji Y, Recombination centres and the orchestration of V(D)J recombination. Nat Rev Immunol 11, 251–263 (2011). [PubMed: 21394103]
4. Cobb RM, Oestreich KJ, Osipovich OA, Oltz EM, Accessibility control of V(D)J recombination. Adv. Immunol. 91, 45–109 (2006). [PubMed: 16938538]
5. Kim M-S, Lapkouski M, Yang W, Gellert M, Crystal structure of the V(D)J recombinase RAG1-RAG2. Nature 518, 507–511 (2015). [PubMed: 25707801]
6. Ru H, Chambers MG, Fu T-M, Tong AB, Liao M, Wu H, Molecular Mechanism of V(D)J Recombination from Synaptic RAG1-RAG2 Complex Structures. Cell 163, 1138–1152 (2015). [PubMed: 26548953]
7. Bolland DJ, Wood AL, Johnston CM, Bunting SF, Morgan G, Chakalova L, Fraser PJ, Corcoran AE, Antisense intergenic transcription in V(D)J recombination. Nat Immunol 5, 630–637 (2004). [PubMed: 15107847]
8. Bolland DJ, Wood AL, Afshar R, Featherstone K, Oltz EM, Corcoran AE, Antisense intergenic transcription precedes Igh D-to-J recombination and is controlled by the intronic enhancer Emu. Mol Cell Biol 27, 5523–5533 (2007). [PubMed: 17526723]
9. Yancopoulos GD, Alt FW, Developmentally controlled and tissue-specific expression of unrearranged VH gene segments. Cell 40, 271–281 (1985). [PubMed: 2578321]
10. Laffleur B, Lim J, Zhang W, Chen Y, Pefanis E, Bizarro J, Batista CR, Wu L, Economides AN, Wang J, Basu U, Noncoding RNA processing by DIS3 regulates chromosomal architecture and somatic hypermutation in B cells. Nat Genet 53, 230–242 (2021). [PubMed: 33526923]
11. Dai H-Q, Hu H, Lou J, Ye AY, Ba Z, Zhang X, Zhang Y, Zhao L, Yoon HS, Chapdelaine-Williams AM, Kyritsis N, Chen H, Johnson K, Lin S, Conte A, Casellas R, Lee C-S, Alt FW, Loop extrusion mediates physiological Igh locus contraction for RAG scanning. Nature 590, 338–343 (2021). [PubMed: 33442057]
12. Zhang Y, Zhang X, Ba Z, Liang Z, Dring EW, Hu H, Lou J, Kyritsis N, Zurita J, Shamim MS, Presser Aiden A, Lieberman Aiden E, Alt FW, The fundamental role of chromatin loop extrusion in physiological V(D)J recombination. Nature 573, 600–604 (2019). [PubMed: 31511698]
13. Hill L, Ebert A, Jaritz M, Wutz G, Nagasaka K, Tagoh H, Kostanova-Poliakova D, Schindler K, Sun Q, Bönelt P, Fischer M, Peters J-M, Busslinger M, Wapl repression by Pax5 promotes V gene recombination by Igh loop extrusion. Nature 584, 142–147 (2020). [PubMed: 32612238]
14. Brecht RM, Liu CC, Beilinson HA, Khitun A, Slavoff SA, Schatz DG, Nucleolar localization of RAG1 modulates V(D)J recombination activity. PNAS 117, 4300–4309 (2020). [PubMed: 32047031]
15. Kilchert C, Wittmann S, Vasiljeva L, The regulation and functions of the nuclear RNA exosome complex. Nature Reviews Molecular Cell Biology 17, 227–239 (2016). [PubMed: 26726035]
16. Nair L, Chung H, Basu U, Regulation of long non-coding RNAs and genome dynamics by the RNA surveillance machinery. Nat Rev Mol Cell Biol 21, 123–136 (2020). [PubMed: 32020081]
17. Liu J, Dou X, Chen C, Chen C, Liu C, Xu MM, Zhao S, Shen B, Gao Y, Han D, He C, N6-methyladenosine of chromosome-associated regulatory RNA regulates chromatin state and transcription. Science 367, 580–586 (2020). [PubMed: 31949099]
18. Chapman MA, Lawrence MS, Keats JJ, Cibulskis K, Sougnez C, Schinzel AC, Harview CL, Brunet J-P, Ahmann GJ, Adli M, Anderson KC, Ardlie KG, Auclair D, Baker A, Bergsagel PL, Bernstein BE, Drier Y, Fonseca R, Gabriel SB, Hofmeister CC, Jagannath S, Jakubowiak AJ, Krishnan A, Levy J, Liefeld T, Lonial S, Mahan S, Mfuko B, Monti S, Perkins LM, Onofrio R, Pugh TJ, Rajkumar SV, Ramos AH, Siegel DS, Sivachenko A, Stewart AK, Trudel S, Vij R, Voet D, Winckler W, Zimmerman T, Carpten J, Trent J, Hahn WC, Garraway LA, Meyerson M, Lander ES, Getz G, Golub TR, Initial genome sequencing and analysis of multiple myeloma. Nature 471, 467–472 (2011). [PubMed: 21430775]

19. Walker BA, Mavrommatis K, Wardell CP, Ashby TC, Bauer M, Davies FE, Rosenthal A, Wang H, Qu P, Hoering A, Samur M, Towfic F, Ortiz M, Flynt E, Yu Z, Yang Z, Rozelle D, Obenauer J, Trotter M, Auclair D, Keats J, Bolli N, Fulciniti M, Szalat R, Moreau P, Durie B, Stewart AK, Goldschmidt H, Raab MS, Einsele H, Sonneveld P, San Miguel J, Lonial S, Jackson GH, Anderson KC, Avet-Loiseau H, Munshi N, Thakurta A, Morgan GJ, Identification of novel mutational drivers reveals oncogene dependencies in multiple myeloma. Blood, blood-2018–03-840132 (2018).
20. Fabre A, Charroux B, Martinez-Vinson C, Roquelaure B, Odul E, Sayar E, Smith H, Colomb V, Andre N, Hugot J-P, Goulet O, Lacoste C, Sarles J, Royet J, Levy N, Badens C, SKIV2L mutations cause syndromic diarrhea, or trichohepatoenteric syndrome. Am J Hum Genet 90, 689–692 (2012). [PubMed: 22444670]
21. Basu U, Meng F-L, Keim C, Grinstein V, Pefanis E, Eccleston J, Zhang T, Myers D, Wasserman CR, Wesemann DR, Januszyk K, Gregory RI, Deng H, Lima CD, Alt FW, The RNA exosome targets the AID cytidine deaminase to both strands of transcribed duplex DNA substrates. Cell 144, 353–363 (2011). [PubMed: 21255825]
22. Lim J, Giri PK, Kazadi D, Laffleur B, Zhang W, Grinstein V, Pefanis E, Brown LM, Ladewig E, Martin O, Chen Y, Rabadan R, Boyer F, Rothschild G, Cogné M, Pinaud E, Deng H, Basu U, Nuclear Proximity of Mtr4 to RNA Exosome Restricts DNA Mutational Asymmetry. Cell 169, 523–537.e15 (2017). [PubMed: 28431250]
23. Methot SP, Di Noia JM, Molecular Mechanisms of Somatic Hypermutation and Class Switch Recombination. Adv. Immunol. 133, 37–87 (2017). [PubMed: 28215280]
24. Pefanis E, Wang J, Rothschild G, Lim J, Chao J, Rabadan R, Economides AN, Basu U, Noncoding RNA transcription targets AID to divergently transcribed loci in B cells. Nature 514, 389–393 (2014). [PubMed: 25119026]
25. Pefanis E, Wang J, Rothschild G, Lim J, Kazadi D, Sun J, Federation A, Chao J, Elliott O, Liu Z-P, Economides AN, Bradner JE, Rabadan R, Basu U, RNA exosome-regulated long non-coding RNA transcription controls super-enhancer activity. Cell 161, 774–789 (2015). [PubMed: 25957685]
26. Hobeika E, Thiemann S, Storch B, Jumaa H, Nielsen PJ, Pelanda R, Reth M, Testing gene function early in the B cell lineage in mb1-cre mice. PNAS 103, 13789–13794 (2006). [PubMed: 16940357]
27. Singh I, Contreras A, Cordero J, Rubio K, Dobersch S, Günther S, Jeratsch S, Mehta A, Krüger M, Graumann J, Seeger W, Dobreva G, Braun T, Barreto G, MiCEE is a ncRNA-protein complex that mediates epigenetic silencing and nucleolar organization. Nat Genet 50, 990–1001 (2018). [PubMed: 29867223]
28. Guidos CJ, Williams CJ, Grandal I, Knowles G, Huang MT, Danska JS, V(D)J recombination activates a p53-dependent DNA damage checkpoint in scid lymphocyte precursors. Genes Dev. 10, 2038–2054 (1996). [PubMed: 8769647]
29. Shinkai Y, Koyasu S, Nakayama K, Murphy KM, Loh DY, Reinherz EL, Alt FW, Restoration of T cell development in RAG-2-deficient mice by functional TCR transgenes. Science 259, 822–825 (1993). [PubMed: 8430336]
30. Shih T-AY, Roederer M, Nussenzweig MC, Role of antigen receptor affinity in T cell-independent antibody responses in vivo. Nat. Immunol. 3, 399–406 (2002). [PubMed: 11896394]
31. Choi YS, Baumgarth N, Dual role for B-1a cells in immunity to influenza virus infection. J Exp Med 205, 3053–3064 (2008). [PubMed: 19075288]
32. Molleston JM, Sabin LR, Moy RH, Menghani SV, Rausch K, Gordesky-Gold B, Hopkins KC, Zhou R, Jensen TH, Wilusz JE, Cherry S, A conserved virus-induced cytoplasmic TRAMP-like complex recruits the exosome to target viral RNA for degradation. Genes Dev 30, 1658–1670 (2016). [PubMed: 27474443]
33. Niiro H, Clark EA, Regulation of B-cell fate by antigen-receptor signals. Nat. Rev. Immunol. 2, 945–956 (2002). [PubMed: 12461567]
34. Marquet M, Garot A, Bender S, Carrion C, Rouaud P, Lecardeur S, Denizot Y, Cogné M, Pinaud E, The Eμ enhancer region influences H chain expression and B cell fate without impacting IgVH repertoire and immune response in vivo. J. Immunol. 193, 1171–1183 (2014). [PubMed: 24965776]

35. Sarma K, Cifuentes-Rojas C, Ergun A, del Rosario A, Jeon Y, White F, Sadreyev R, Lee JT, ATRX Directs Binding of PRC2 to Xist RNA and Polycomb Targets. Cell 159, 869–883 (2014). [PubMed: 25417162]
36. Sun J, Keim CD, Wang J, Kazadi D, Oliver PM, Rabadan R, Basu U, E3-ubiquitin ligase Nedd4 determines the fate of AID-associated RNA polymerase II in B cells. Genes Dev 27, 1821–1833 (2013). [PubMed: 23964096]
37. Wang X, Paucek RD, Gooding AR, Brown ZZ, Ge EJ, Muir TW, Cech TR, Molecular analysis of PRC2 recruitment to DNA in chromatin and its inhibition by RNA. Nat Struct Mol Biol 24, 1028–1038 (2017). [PubMed: 29058709]
38. Yang F, Tanasa B, Micheletti R, Ohgi KA, Aggarwal AK, Rosenfeld MG, Shape of promoter antisense RNAs regulates ligand-induced transcription activation. Nature 595, 444–449 (2021). [PubMed: 34194047]
39. Rothschild G, Zhang W, Lim J, Giri PK, Laffleur B, Chen Y, Fang M, Chen Y, Nair L, Liu Z-P, Deng H, Hammarström L, Wang J, Basu U, Noncoding RNA transcription alters chromosomal topology to promote isotype-specific class switch recombination. Sci Immunol 5, eaay5864 (2020). [PubMed: 32034089]
40. Kim T-K, Hemberg M, Gray JM, Costa AM, Bear DM, Wu J, Harmin DA, Laptewicz M, Barbara-Haley K, Kuersten S, Markenscoff-Papadimitriou E, Kuhl D, Bito H, Worley PF, Kreiman G, Greenberg ME, Widespread transcription at neuronal activity-regulated enhancers. Nature 465, 182–187 (2010). [PubMed: 20393465]
41. Andrulis ED, Werner J, Nazarian A, Erdjument-Bromage H, Tempst P, Lis JT, The RNA processing exosome is linked to elongating RNA polymerase II in Drosophila. Nature 420, 837–841 (2002). [PubMed: 12490954]
42. Lemay J-F, Larochelle M, Marguerat S, Atkinson S, Bähler J, Bachand F, The RNA exosome promotes transcription termination of backtracked RNA polymerase II. Nat Struct Mol Biol 21, 919–926 (2014). [PubMed: 25240800]
43. Bolland DJ, Koohy H, Wood AL, Matheson LS, Krueger F, Stubbington MJT, Baizan-Edge A, Chovanec P, Stubbs BA, Tabbada K, Andrews SR, Spivakov M, Corcoran AE, Two Mutually Exclusive Local Chromatin States Drive Efficient V(D)J Recombination. Cell Rep 15, 2475–2487 (2016). [PubMed: 27264181]
44. Matheson LS, Bolland DJ, Chovanec P, Krueger F, Andrews S, Koohy H, Corcoran AE, Local Chromatin Features Including PU.1 and IKAROS Binding and H3K4 Methylation Shape the Repertoire of Immunoglobulin Kappa Genes Chosen for V(D)J Recombination. Front Immunol 8, 1550 (2017). [PubMed: 29204143]
45. Pulivarthy SR, Lion M, Kuzu G, Matthews AGW, Borowsky ML, Morris J, Kingston RE, Dennis JH, Tolstorukov MY, Oettinger MA, Regulated large-scale nucleosome density patterns and precise nucleosome positioning correlate with V(D)J recombination. Proc Natl Acad Sci U S A 113, E6427–E6436 (2016). [PubMed: 27698124]
46. Angelin-Duclos C, Calame K, Evidence that immunoglobulin VH-DJ recombination does not require germ line transcription of the recombining variable gene segment. Mol. Cell. Biol. 18, 6253–6264 (1998). [PubMed: 9774642]
47. Du H, Ishii H, Pazin MJ, Sen R, Activation of 12/23-RSS-dependent RAG cleavage by hSWI/SNF complex in the absence of transcription. Mol. Cell 31, 641–649 (2008). [PubMed: 18775324]
48. Oudinet C, Braikia F-Z, Dauba A, Khamlichi AA, Recombination may occur in the absence of transcription in the immunoglobulin heavy chain recombination centre. Nucleic Acids Res. (2020), doi:10.1093/nar/gkaa108.
49. Domingo-Prim J, Endara-Coll M, Bonath F, Jimeno S, Prados-Carvajal R, Friedländer MR, Huertas P, Visa N, EXOSC10 is required for RPA assembly and controlled DNA end resection at DNA double-strand breaks. Nat Commun 10, 2135 (2019). [PubMed: 31086179]
50. Yang Kun, Han Jie, Gill Jennifer, Park Jason, Sathe Meghana N., Gattineni Jyothsna, Wright Tracey, Wysocki Christian, Teresa de la Morena, Nan Yan, Trichohepatoenteric syndrome-associated mutation in SKIV2L blocks early B cell developmentScience Immunology.

51. Tuck AC, Rankova A, Arpat AB, Liechti LA, Hess D, Iesmantavicius V, Castelo-Szekely V, Gatfield D, Bühler M, Mammalian RNA Decay Pathways Are Highly Specialized and Widely Linked to Translation. Molecular Cell 77, 1222–1236.e13 (2020). [PubMed: 32048998]
52. Zinoviev A, Ayupov RK, Abaeva IS, Hellen CUT, Pestova TV, Extraction of mRNA from Stalled Ribosomes by the Ski Complex. Molecular Cell 77, 1340–1349.e6 (2020). [PubMed: 32006463]
53. Kögel A, Keidel A, Bonneau F, Schäfer IB, Conti E, The human SKI complex regulates channeling of ribosome-bound RNA to the exosome via an intrinsic gatekeeping mechanism. Mol Cell 82, 756–769.e8 (2022). [PubMed: 35120588]
54. Puno MR, Lima CD, Structural basis for MTR4–ZCCHC8 interactions that stimulate the MTR4 helicase in the nuclear exosome-targeting complex. Proceedings of the National Academy of Sciences 115, E5506–E5515 (2018).
55. Fuxa M, Skok J, Souabni A, Salvagiotto G, Roldan E, Busslinger M, Pax5 induces V-to-DJ rearrangements and locus contraction of the immunoglobulin heavy-chain gene. Genes Dev 18, 411–422 (2004). [PubMed: 15004008]
56. Rouaud P, Vincent-Fabert C, Saintamand A, Fiancette R, Marquet M, Robert I, Reina-San-Martin B, Pinaud E, Cogné M, Denizot Y, The IgH 3' regulatory region controls somatic hypermutation in germinal center B cells. J. Exp. Med. 210, 1501–1507 (2013). [PubMed: 23825188]
57. Corces MR, Trevino AE, Hamilton EG, Greenside PG, Sinnott-Armstrong NA, Vesuna S, Satpathy AT, Rubin AJ, Montine KS, Wu B, Kathiria A, Cho SW, Mumbach MR, Carter AC, Kasowski M, Orloff LA, Risca VI, Kundaje A, Khavari PA, Montine TJ, Greenleaf WJ, Chang HY, An improved ATAC-seq protocol reduces background and enables interrogation of frozen tissues. Nature Methods 14, 959–962 (2017). [PubMed: 28846090]
58. Kim D, Langmead B, Salzberg SL, HISAT: a fast spliced aligner with low memory requirements. Nat Methods 12, 357–360 (2015). [PubMed: 25751142]
59. Pertea M, Pertea GM, Antonescu CM, Chang T-C, Mendell JT, Salzberg SL, StringTie enables improved reconstruction of a transcriptome from RNA-seq reads. Nat Biotechnol 33, 290–295 (2015). [PubMed: 25690850]
60. Huang DW, Sherman BT, Lempicki RA, Systematic and integrative analysis of large gene lists using DAVID bioinformatics resources. Nat Protoc 4, 44–57 (2009). [PubMed: 19131956]
61. Song L, Cohen D, Ouyang Z, Cao Y, Hu X, Liu XS, TRUST4: immune repertoire reconstruction from bulk and single-cell RNA-seq data. Nat Methods 18, 627–630 (2021). [PubMed: 33986545]
62. Martin M, Cutadapt removes adapter sequences from high-throughput sequencing reads. EMBnet.journal 17, 10–12 (2011).
63. Langmead B, Salzberg SL, Fast gapped-read alignment with Bowtie 2. Nat Methods 9, 357–359 (2012). [PubMed: 22388286]
64. Zhang Y, Liu T, Meyer CA, Eeckhoute J, Johnson DS, Bernstein BE, Nusbaum C, Myers RM, Brown M, Li W, Liu XS, Model-based Analysis of ChIP-Seq (MACS). Genome Biology 9, R137 (2008). [PubMed: 18798982]

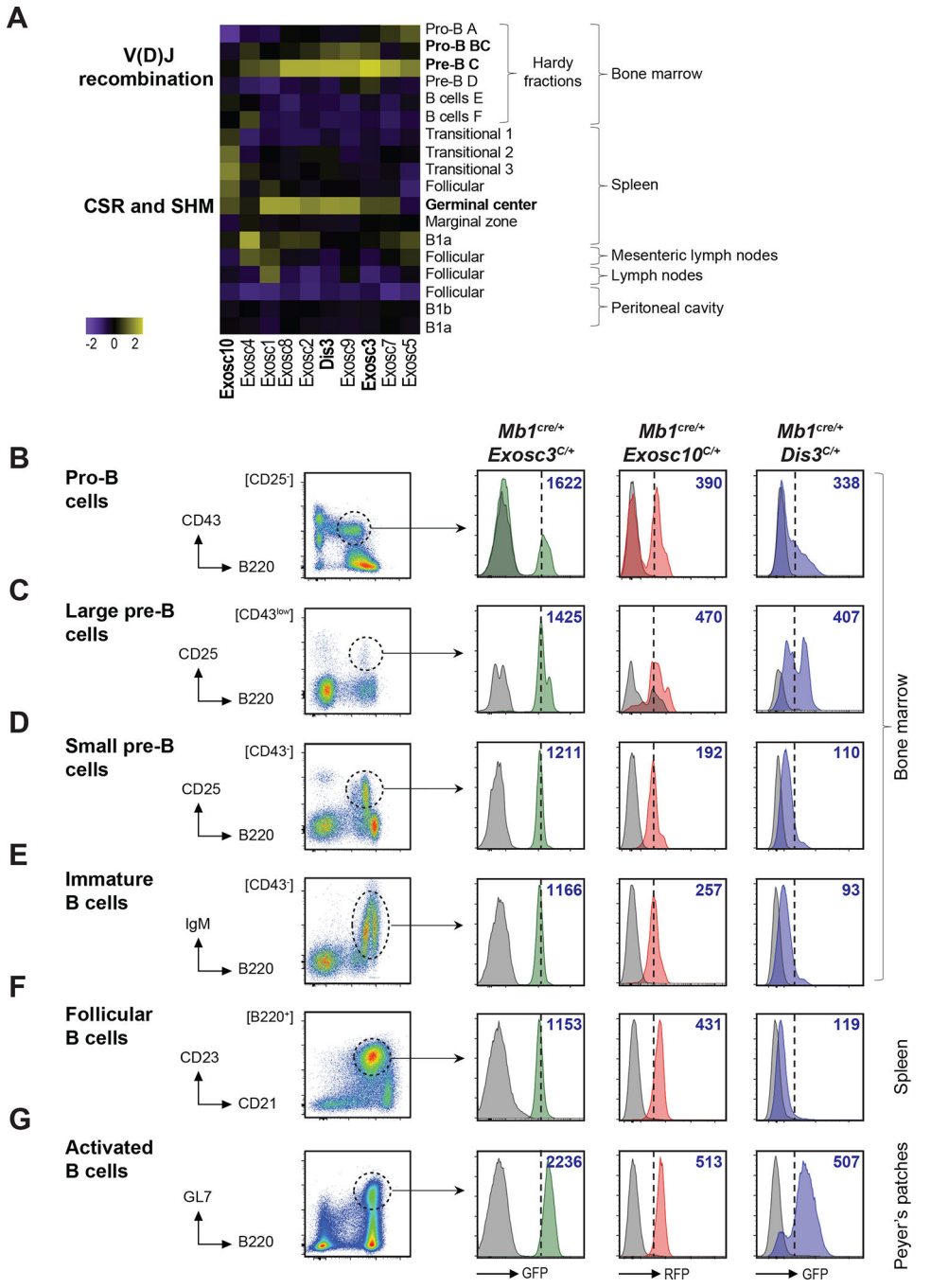

Fig. 1. Dynamic RNA exosome subunits expression during B cell development.

(**A**) Heat map showing RNA exosome subunit expression in mouse B cells, data were obtained from "ImmGen" databank. Relative transcriptomic expression of the RNA exosome subunits is shown in the main B cell populations from various lymphoid organs in adult mice. (**B to G**) Flow cytometry analysis of *Mb1*$^{cre/+}$ *Exosc3*$^{COIN/+}$, *Mb1*$^{cre/+}$ *Exosc10*$^{COIN/+}$ and *Mb1*$^{cre/+}$ *Dis3*$^{COIN/+}$ B cell populations. Cells were collected form bone marrow, spleen and Peyer's patches and the B cell populations were identified as: (**B**) pro-B cells (CD43^{+}, B220^{+}, CD25^{-}, IgM^{-}), (**C**) large pre-B cells (FSC-A^{high}, CD43^{low}, B220^{+}, CD25^{low}),

(**D**) small pre-B cells ($CD43^{-}$, $B220^{+}$, $CD25^{+}$, IgM^{-}), (**E**) immature B cells ($CD43^{-}$, $B220^{+}$, $CD25^{-}$, IgM^{+}), (**F**) follicular B cells ($B220^{+}$ $CD23^{+}$ $CD21^{dim}$), and (**G**) activated B cells ($B220^{+}$, $GL7^{+}$). GFP or RFP expression is shown in each subpopulation after specific gating. *Mb1*$^{cre/+}$ mice were used as control for GFP/RFP expression, show as grey histograms. The dashed line represents the threshold for high GFP/RFP expression. Mean fluorescent intensities (MFI) of GFP^{+}/RFP^{+} cells are indicated in blue (see also Fig. S1F–S1H). These data are representative from at least 3 independent experiments per genotype, using a total of at least 3 mice per group.

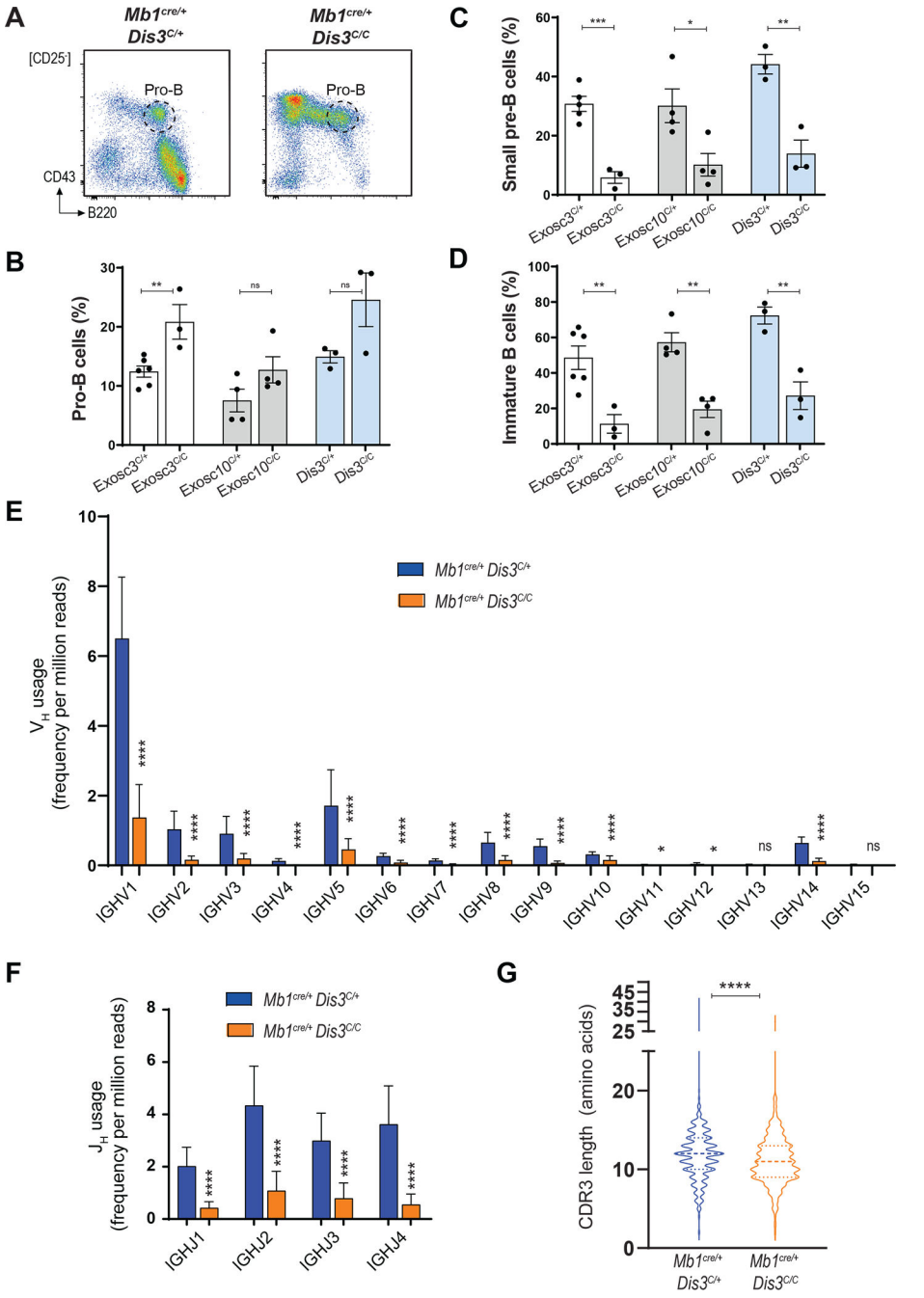

Fig. 2. RNA exosome is mandatory for early B cell development and *Igh* recombination.

(**A**) Flow cytometry analysis of bone marrow pro-B cell populations from *Mb1*$^{cre/+}$ *Dis3*$^{C/+}$ and *Mb1*$^{cre/+}$ *Dis3*$^{C/C}$ mice. (**B**) Quantification of bone marrow pro-B cells (CD43^{+}, B220^{+}, CD25^{-}, IgM^{-}), from *Mb1*$^{cre/+}$ *Exosc3*$^{C/+}$, *Mb1*$^{cre/+}$ *Exosc3*$^{C/C}$, *Mb1*$^{cre/+}$ *Exosc10*$^{C/+}$, *Mb1*$^{cre/+}$ *Exosc10*$^{C/C}$, *Mb1*$^{cre/+}$ *Dis3*$^{C/+}$ and *Mb1*$^{cre/+}$ *Dis3*$^{C/C}$ mice. (**C**) Quantification of bone marrow small pre-B cells (CD43^{-}, B220^{+}, CD25^{+}, IgM^{-}). (**D**) Quantification of bone marrow immature B cells (CD43^{-}, B220^{+}, CD25^{-}, IgM^{+}). These results are representative from at least 3 independent experiments, using a total of at least 3 mice per group. Bar graphs show mean value +/− SEM, analyzed with two-tailed unpaired *t*-test. (**E**) V_H

repertoire in *Mb1*$^{cre/+}$ *Dis3*$^{C/+}$ and *Mb1*$^{cre/+}$ *Dis3*$^{C/C}$ pro-B cells. Mean is shown, +/− SEM. (**F**) J_H repertoire in *Mb1*$^{cre/+}$ *Dis3*$^{C/+}$ and *Mb1*$^{cre/+}$ *Dis3*$^{C/C}$ pro-B cells. Mean is shown, +/− SEM. The V(D)J repertoire was determined by RNA-sequencing of pro-B cells (3 independent experiments), and the number of productive V(D)J rearrangements compared to the total number of reads was used to perform statistical analyses (khi2 proportion test). (**G**) CDR3 length was analyzed and the violin plots show their distribution in the presence or absence of DIS3 (two-tailed unpaired *t*-test on combined data from 3 mice).

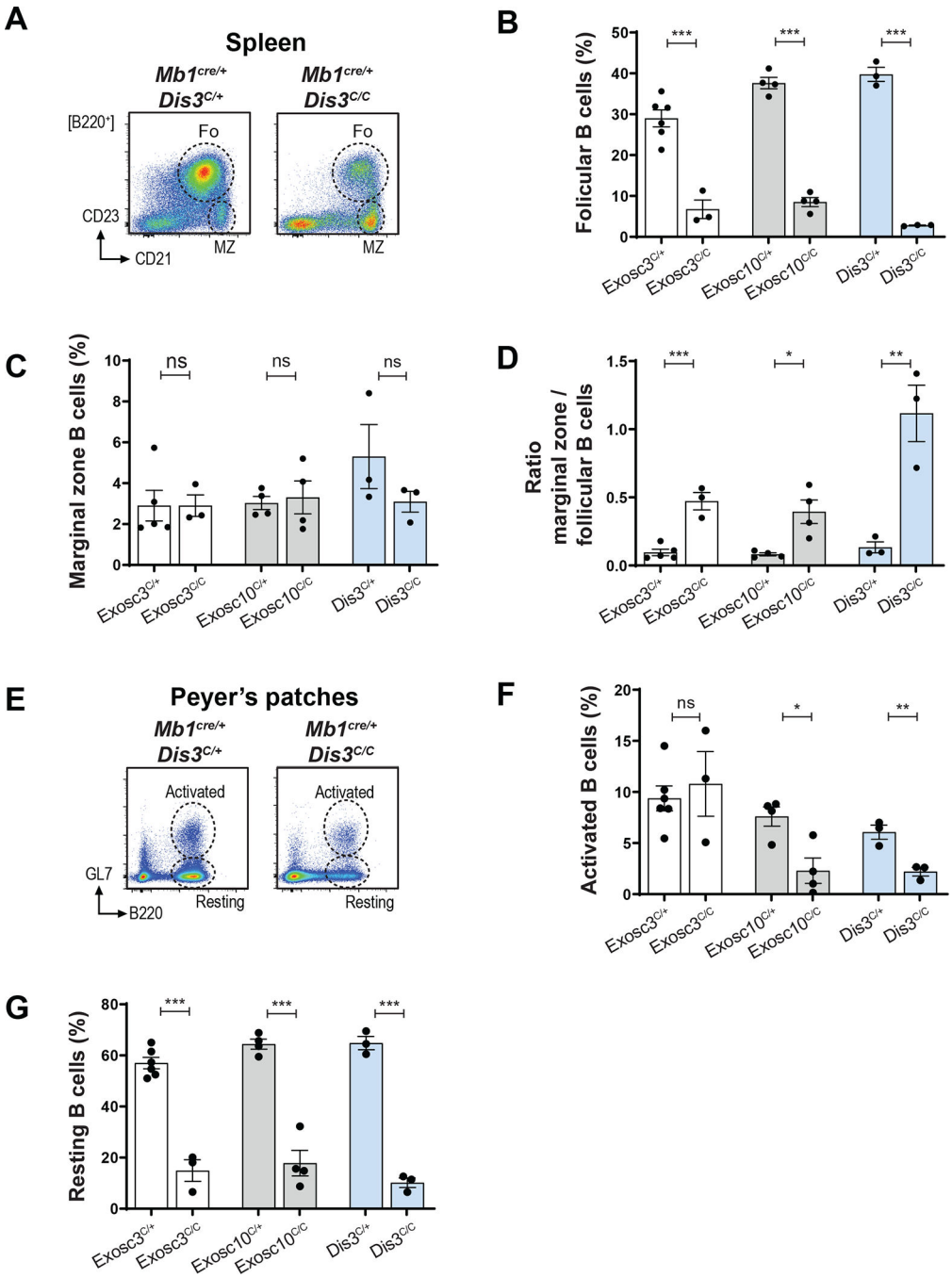

Fig. 3: RNA exosome affects mature B cell development.

(**A**) Flow cytometry analysis of spleen B cell populations from *Mb1*$^{cre/+}$ *Dis3*$^{C/+}$ and *Mb1*$^{cre/+}$ *Dis3*$^{C/C}$ mice. Fo = follicular B cells, MZ = marginal zone B cells. (**B**) Quantification of spleen follicular B cells (B220^{+} CD23^{+} CD21^{dim}). Data from *Mb1*$^{cre/+}$ *Exosc3*$^{C/+}$, *Mb1*$^{cre/+}$ *Exosc3*$^{C/C}$, *Mb1*$^{cre/+}$ *Exosc10*$^{C/+}$, *Mb1*$^{cre/+}$ *Exosc10*$^{C/C}$, *Mb1*$^{cre/+}$ *Dis3*$^{C/+}$ and *Mb1*$^{cre/+}$ *Dis3*$^{C/C}$ mice are shown. (**C**) Quantification of spleen marginal zone B cells (B220^{+} CD23^{-} CD21^{+}). Data from *Mb1*$^{cre/+}$ *Exosc3*$^{C/+}$, *Mb1*$^{cre/+}$ *Exosc3*$^{C/C}$, *Mb1*$^{cre/+}$ *Exosc10*$^{C/+}$, *Mb1*$^{cre/+}$ *Exosc10*$^{C/C}$, *Mb1*$^{cre/+}$ *Dis3*$^{C/+}$ and *Mb1*$^{cre/+}$ *Dis3*$^{C/C}$ mice

are shown. (**D**) The ratios of marginal zone / follicular B cells (Fig. 3C, 3D) were quantified from these mice. (**E**) Flow cytometry analysis of Peyer's patches B cell populations from *Mb1*$^{cre/+}$ *Dis3*$^{C/+}$ and *Mb1*$^{cre/+}$ *Dis3*$^{C/C}$ mice. (**F**) Quantification of Peyer's patches resting B cells (B220^{+} GL7^{-}). Data were obtained from *Mb1*$^{cre/+}$ *Exosc10*$^{C/+}$, *Mb1*$^{cre/+}$ *Exosc10*$^{C/C}$, *Mb1*$^{cre/+}$ *Dis3*$^{C/+}$ and *Mb1*$^{cre/+}$ *Dis3*$^{C/C}$ mice. (**G**) Quantification of Peyer's patches activated B cells (B220^{+} GL7^{+}). Data were obtained from *Mb1*$^{cre/+}$ *Exosc10*$^{C/+}$, *Mb1*$^{cre/+}$ *Exosc10*$^{C/C}$, *Mb1*$^{cre/+}$ *Dis3*$^{C/+}$ and *Mb1*$^{cre/+}$ *Dis3*$^{C/C}$ mice. These results are representative from at least 3 independent experiments, using a total of at least 3 mice per group. Bar graphs show mean value +/− SEM, analyzed with two-tailed unpaired *t*-test.

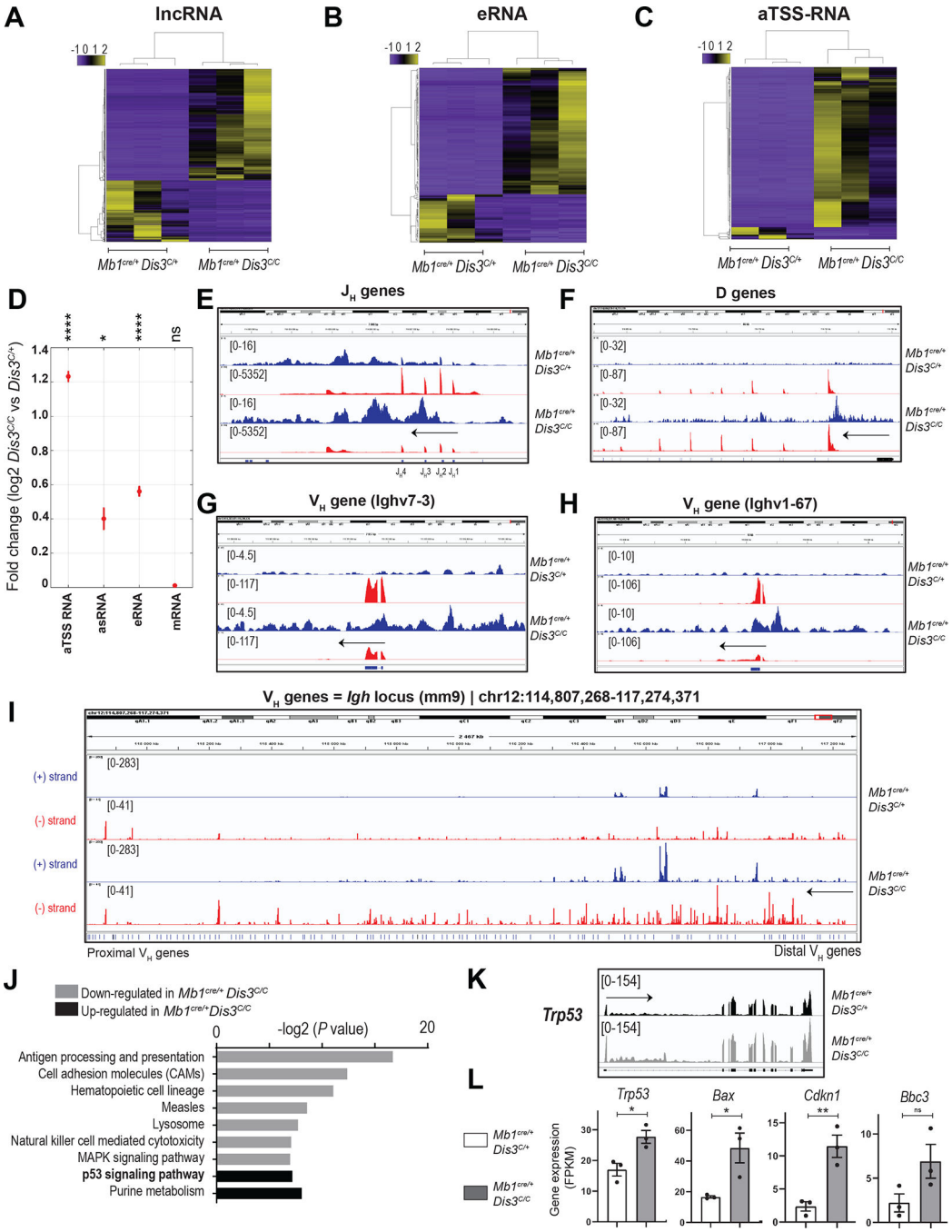

Fig. 4. RNA-sequencing reveals RNA exosome substrates from pro-B cells *in vivo*.

RNA-sequencing of pro-B cells from *Mb1*$^{cre/+}$ *Dis3*$^{C/+}$ and *Mb1*$^{cre/+}$ *Dis3*$^{C/C}$ mice. (**A**) Heat map showing the lncRNAs upregulated (in yellow, 2544) and downregulated (purple, 1405) in the absence of DIS3. (**B**) Heat map showing the eRNAs upregulated (157) and downregulated (60) in the absence of DIS3. (**C**) Heat map showing the aTSS-RNAs upregulated (461) and downregulated (35) in the absence of DIS3. Unsupervised hierarchical clustering is shown. (**D**) Genome-wide analysis of DIS3-sensitive RNA substrates in pro-B cells *in vivo*. The fold increase for the different classes of non-coding

RNAs is shown, including antisense transcription start site associated RNAs (aTSS RNA), antisense RNAs (asRNA), enhancer RNAs (eRNAs), and messenger RNAs (mRNA), Wilcoxon rank sum test. (**E to I**) 3 independent RNA-sequencing experiments were performed showing similar results. The data were combined for a better visualization using the IGV viewer and to present the RNA tracks. Owing to strand specific sequencing, + (blue) tracks represent the RNA corresponding to the Watson DNA strand and – (red) tracks represent the RNA corresponding to the Crick DNA strand, black arrows indicate the direction of coding transcription. (**E**) Accumulation of non-coding RNAs at the J_H1 to J_H4 genes region in the absence of RNA exosome activity. (**F**) Accumulation of non-coding RNAs at the D genes region in the absence of RNA exosome activity. (**G**) Example of non-coding RNA accumulation at V_H (Ighv7–3) gene in the absence of RNA exosome activity, while coding gene expression is decreased. (**H**) Example of non-coding RNA accumulation at V_H (Ighv1–67) gene in the absence of RNA exosome activity, while coding gene expression is decreased. (**I)** Non-coding RNA accumulation at the *Igh* locus in DIS3-deficient pro-B cells. The *Igh* locus is shown from the first to the last V_H genes. Sense (red) and antisense (blue) ncRNAs are shown in $Mb1^{cre/+}$ $Dis3^{C/+}$ and $Mb1^{cre/+}$ $Dis3^{C/C}$ pro-B cells, these tracks represent ncRNAs only, after removal of V_H coding transcripts. (**J**) Gene set enrichment analyses are shown from these lists of differentially expressed genes. The downregulated (grey) and upregulated (black) KEGG pathways are shown. (**K**) *Trp53* expression in the absence of DIS3. (**L**) Over-expression of *Trp53* and associated genes in the absence of DIS3 (two-tailed unpaired *t*-test).

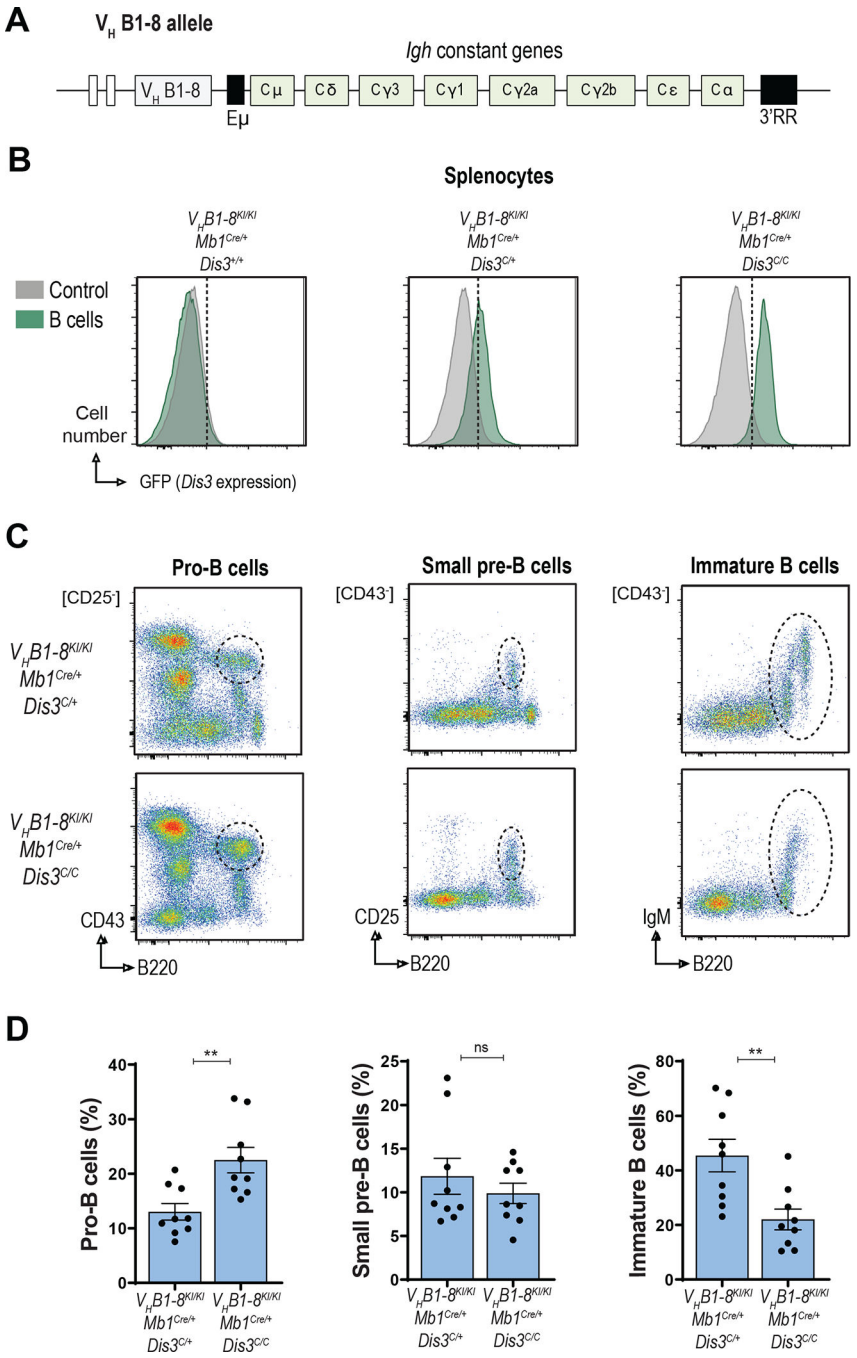

Fig. 5: Introduction of a pre-arranged V(D)J gene restores pre-B cell population.

(**A**) Schematic of the $V_HB1–8$ *knock-in* ($V_HB1–8^{KI}$) allele. $Mb1^{cre/+}$ $Dis3^{COIN}$ mice were crossed with $V_HB1–8^{KI}$ mice to generate the $V_HB1–8^{KI/KI}$ $Mb1^{cre/+}$ $Dis3^{C/+}$ and $V_HB1–8^{KI/KI}$ $Mb1^{cre/+}$ $Dis3^{C/C}$ mouse models. (**B**) Representative FACS plots showing the GFP expression (i.e. *Dis3* expression) from $V_HB1–8^{KI/KI}$ $Mb1^{cre/+}$ $Dis3^{+/+}$, $V_HB1–8^{KI/KI}$ $Mb1^{cre/+}$ $Dis3^{C/+}$ and $V_HB1–8^{KI/KI}$ $Mb1^{cre/+}$ $Dis3^{C/C}$ cells. The grey histograms represent GFP expression in control cells ($B220^-$) while the green histograms show GFP expression in B cells ($B220^+$ Igk^+). (**C**) Flow cytometry analyses of bone marrow pro-B cells ($CD43^+$,

B220^{+}, CD25^{-}, IgM^{-}), small pre-B cells (CD43^{-}, B220^{+}, CD25^{+}, IgM^{-}) and immature B cells (CD43^{-}, B220^{+}, CD25^{-}, IgM^{+}) populations from $V_HB1\text{–}8^{KI/KI}$ $Mb1^{cre/+}$ $Dis3^{C/+}$ and $V_HB1\text{–}8^{KI/KI}$ $Mb1^{cre/+}$ $Dis3^{C/C}$ mice. (**D**) Quantification of bone marrow pro-B, small pre-B, and immature B cell populations from $V_HB1\text{–}8^{KI/KI}$ $Mb1^{cre/+}$ $Dis3^{C/+}$ and $V_HB1\text{–}8^{KI/KI}$ $Mb1^{cre/+}$ $Dis3^{C/C}$ mice. These results are representative from 6 independent experiments, using a total of 9 mice per group. Bar graphs show mean value +/− SEM, analyzed with two-tailed unpaired *t*-test.

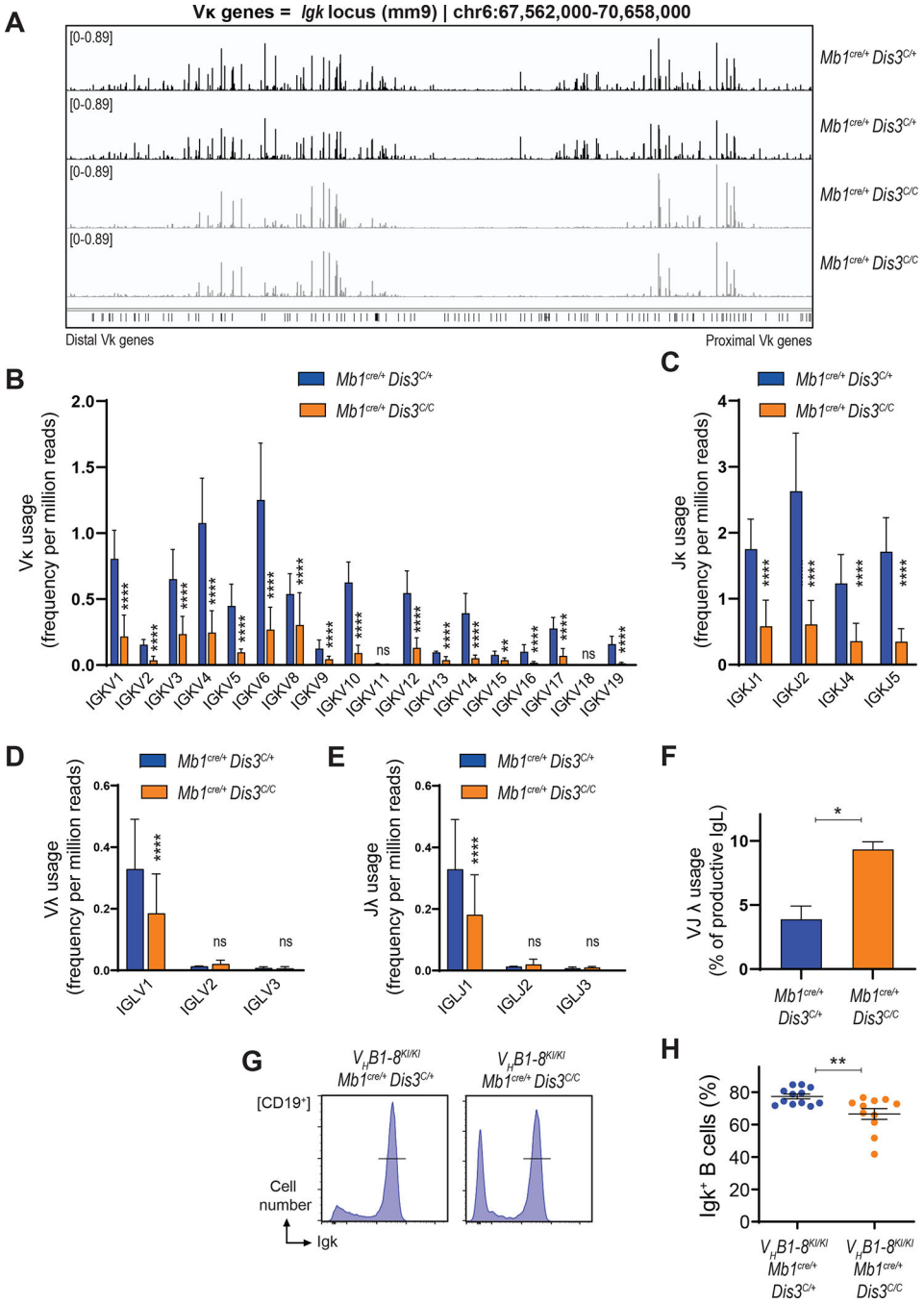

Fig. 6: Chromatin accessibility in the absence of RNA processing.

(**A**) ATAC-seq experiments were performed on pro-B cells from *Mb1*$^{cre/+}$ *Dis3*$^{C/+}$ and *Mb1*$^{cre/+}$ *Dis3*$^{C/C}$ mice, accessibility of *Vk* genes is shown (2 independent experiments). (**B**) *Vk* repertoire in *Mb1*$^{cre/+}$ *Dis3*$^{C/+}$ and *Mb1*$^{cre/+}$ *Dis3*$^{C/C}$ pro-B cells. (**C**) *Jk* repertoire in *Mb1*$^{cre/+}$ *Dis3*$^{C/+}$ and *Mb1*$^{cre/+}$ *Dis3*$^{C/C}$ pro-B cells. (**D**) *Vλ* repertoire in *Mb1*$^{cre/+}$ *Dis3*$^{C/+}$ and *Mb1*$^{cre/+}$ *Dis3*$^{C/C}$ pro-B cells. (**E**) *Jλ* repertoire in *Mb1*$^{cre/+}$ *Dis3*$^{C/+}$ and *Mb1*$^{cre/+}$ *Dis3*$^{C/C}$ pro-B cells. The VJ repertoire was determined by RNA-sequencing of pro-B cells (3 independent experiments, mean is shown, +/− SEM), and the number of productive

VJ rearrangements compared to the total number of reads was used to perform statistical analyses (khi2 proportion test). (**F**) The number of productive Igλ rearrangements among the total number of productive IgL rearrangements was determined (three independent experiments, two-tailed paired *t*-test). (**G**) Flow cytometry analyses of Igk expression on B splenocytes ($CD19^+$) from $V_HB1\text{–}8^{KI/KI}$ $Mb1^{cre/+}$ $Dis3^{C/+}$ and $V_HB1\text{–}8^{KI/KI}$ $Mb1^{cre/+}$ $Dis3^{C/C}$ mice. (**H**) Quantification of Igk expression on B splenocytes ($CD19^+$) from $V_HB1\text{–}8^{KI/KI}$ $Mb1^{cre/+}$ $Dis3^{C/+}$ and $V_HB1\text{–}8^{KI/KI}$ $Mb1^{cre/+}$ $Dis3^{C/C}$ mice. 6 independent experiments (n=11 to 12 mice), mean is shown +/− SEM, two-tailed unpaired *t*-test.